# Analysis of Predictive Direct Torque Control Applied to Induction Motor by Finite Element Method

**A. S. Lunardi** * **A. J. Sguarezi Filho** ** **A. Pelizari** ** **G. R. Bruzinga** **

* *University of Sao Paulo, SP (e-mail: angelo.lunardi@usp.br)*
** *Federal University of ABC, SP, (e-mail: alfeu.sguarezi@ufabc.edu.br, ademir.pelizari@ufabc.edu.br, gabriel.bruzinga@ufabc.edu.br).*

**Abstract:** This paper focuses on how to make the electromagnetic analyses of an induction motor drive. The induction motor is controlled by a predictive direct torque controller. Using the predictive control which by a cost-function determines the voltage vector among eight switching states from voltage source converter (VSC), making it suitable for the requirements to control the motor. The controller handles the stator flux and the electromagnetic torque with a quiet implementation and pretty adjusts. Regarding the electromagnetic analyses, it will be done by finite element features. The proposed technique will be illustrated by the results, which will provide how the electromagnetic effects occur inside the electrical machine. The conclusion with all the results is that the controller and machine can be operated with no core saturation.

*Keywords:* Finite Element Analysis, Induction motor, Predictive Control, Direct Torque Control

## 1. INTRODUCTION

In the world more than a half mechanical energy is produced by electrical motors, almost all industrial drive use inductions motors (IM). A wide range of applications can use IMs, the IMs simple construction, robustness, low cost, and reliability are reasons to use in industrial (Sahraoui et al., 2008), on another side, alternative generation systems (Vitorino et al., 2011) and smart grids of electric can also use IMs (Sguarezi Filho and Ruppert, 2010; Costa et al., 2014). The IMs are usually found connected directly in an electric power (Holtz, 1994). Electronic power converters are used for IM's to operate in variable speed and they are continuously growing, meanwhile the use of drivers system in DC Motors (DCM) is decreasing in the same time (Silva et al., 2014). Nowadays, it is easily found different methods to control the IMs electromagnetic torque and speed , it has been widely studied (Depenbrock, 1988). The drive systems used for IM's are the vector control strategies which transform the non-linear torque and speed feature into a linear torque and speed rate similar to that on DCMs.

In the 80s decades, at Takahashi and Noguchi (1986a), a new strategy was proposed for controller IM. It uses coordinate transform and proportional-integral (PI) regulators, which are controlled through field orientation (Blaschke, 1972), hysteresis controllers were replaced by this new strategy.

Predictive control is a wide class of controllers which the future behavior of the controlled variables is predicted by a mathematical model of a system that is the focuses of the predictive control. The optimal actuation signal is obtained from the information provided by the mathematical model, according to the optimized criteria already established. The optimization criterion is based on hysteresis predictive control which is used to ensure that the system-controlled variable is within hysteresis limits. Holtz and Stadtfeld (1983) or a deadbeat technique (Altuna et al., 2015), on the other hand, controllers based on trajectory uses a predefined trajectory to force the variables to track the reference signal (Kennel and Linder, 2000). This kind of control can be used for motor drives, for this it is necessary measured variables like the current $\boldsymbol{i}_{1,\alpha\beta}$ , and speed $\omega$. Furthermore, the electrical machine model used to estimate the states that cannot be measured such as the stator and rotor flux $\boldsymbol{\lambda}_{1,\alpha\beta}$, $\boldsymbol{\lambda}_{2,\alpha\beta}$. Then, the future behavior of the variables is predicted by the same model for each control action (Yazdani and Iravani, 2010). In the end, the controller selects the optimum voltage vector to track the reference in the next step. The most important part is the mathematical model of motor because both predictions and estimations depend on it. Predictive control has advantages compare classics controllers, that make it a real option to improve the dynamic of electrical drives for motor (Rodriguez et al., 2004).For motor power control, it is common they operate in condition less than rated values. Consequently, the voltage and current of the source are used to fewer their rated values, that means the ferromagnetic material does not be over-saturated. Although, there is no sure that the behavior of the machine will be the unsaturated condition in which compromise your operation with the power control, therefore the finite element methods can be a powerful tool for motor analysis during the control operation (Fiser and Ferkolj, 2001).

⋆ This study was financed in part by the Coordenação de Aperfeiçoamento de Pessoal de Nível Superior – Brasil (CAPES) – Finance Code 001 - Gabriel Rodrigues Bruzinga

The predictive torque control studied in this paper, is uses the stator current and flux were considered as state variables (Kumar et al., 2010). Also, the finite element methods allow to analyze the predictive control. Simulation results are presented to validate the study and demonstrating its operational capacity.

So, the organization of the paper is first in the Section 2 present the modeling of squirrel cage induction motor, after some simulation results for the control are showed in Section 3, in Section 4 the analysis through finite element method is the object of study. Finally in Section 6 the conclusions are discussed.

## 2. MODELING OF SQUIRREL CAGE INDUCTION MOTOR

### *2.1 Squirrel Cage Induction Motor Model*

The squirrel cage electrical machine, when operate as motor is known as Squirrel Cage Induction Motor, or just SCIM. The electrical machine can be described by a dynamic model that uses differential equations to represent it in a stationary reference frame $\alpha\beta$ axes can be shown mathematically as (1), (2), (3) and (4).

$$\boldsymbol{v}_{1,\alpha\beta} \;=\; R_1\boldsymbol{i}_{1,\alpha\beta} \;+\; \frac{d\boldsymbol{\lambda}_{1,\alpha\beta}}{dt} \tag{1}$$

$$0 \;=\; \boldsymbol{v}_{2,\alpha\beta} \;= R_2\boldsymbol{i}_{2,\alpha\beta} \;+\; \frac{d\boldsymbol{\lambda}_{2,\alpha\beta}}{dt} \;-\; j(N_p\omega_{mec})\boldsymbol{\lambda}_{2,\alpha\beta} \tag{2}$$

$$\boldsymbol{\lambda}_{1,\alpha\beta} \;=\; L_1\boldsymbol{i}_{1,\alpha\beta} \;+\; L_m\boldsymbol{i}_{2,\alpha\beta} \tag{3}$$

$$\boldsymbol{\lambda}_{2,\alpha\beta} \;=\; L_m\boldsymbol{i}_{1,\alpha\beta} \;+\; L_2\boldsymbol{i}_{2,\alpha\beta} \tag{4}$$

Where, $\boldsymbol{v}_{1,\alpha\beta}$ is the stator voltage vector $\alpha\beta$ components, $\boldsymbol{v}_{2,\alpha\beta}$ is the rotor voltage vector $\alpha\beta$ components, $\boldsymbol{i}_{1,\alpha\beta}$ is the stator current vector $\alpha\beta$ components, $\boldsymbol{i}_{2,\alpha\beta}$ is the rotor current vector $\alpha\beta$ components, $\boldsymbol{\lambda}_{1,\alpha\beta}$ is the stator flux vector $\alpha\beta$ components and $\boldsymbol{\lambda}_{2,\alpha\beta}$ is the rotor flux vector $\alpha\beta$ components. There are components of construction in these equations, as $R_1$ is stator electrical resistance, $R_2$ is rotor electrical resistance, $L_1$ is stator inductance $L_2$ is rotor inductance, $L_m$ inductance of magnetizing and $N_p$ is the number of pair of poles. The electromagnetic torque is obtain by (5).

$$T_e \;=\; \frac{3}{2}\,N_p\Im m[\boldsymbol{\lambda}^*_{1,\alpha\beta}\cdot\boldsymbol{i}_{1,\alpha\beta}] \tag{5}$$

Where the superscript $*$ indicates the complex conjugate (Hernandez Navas et al., 2015; Abad et al., 2011). Moreover, the mechanical dynamic can be described by (6), where $T_{mec}$ is the electromagnetic torque.

$$J\frac{d\omega_{mec}}{dt} \;=\; T_e \;-\; T_{mec} \tag{6}$$

### *2.2 Predictive Direct Torque Control*

One of the vector control strategy is the Direct Torque Control (DTC), whcih focuses on control the electromagnetic torque ($T_e$) and the stator flux ($\lambda_1$) by the voltage applied to the stator terminals. The electromagnetic torque can be controlled changing the angle angle ($\theta_{sr}$) between the rotor and stator flux, that is mathematically represented by (7) (Takahashi and Noguchi, 1986b; Rodriguez et al., 2004).

$$T_e \;=\; \frac{3}{2}N_p\frac{L_m}{L_1L_2\sigma}\lambda_1\lambda_2 sin(\theta_{sr}) \tag{7}$$

Equations (8) and (9) is responsible to estimate the stator and rotor flux.

$$\boldsymbol{\lambda}_{1\alpha\beta} = \int(\boldsymbol{v}_{1,\alpha\beta} - R_1\boldsymbol{i}_{1,\alpha\beta})dt \tag{8}$$

$$\boldsymbol{\lambda}_{2\alpha\beta} = \frac{L_2}{L_m}\boldsymbol{\lambda}_{1,\alpha\beta} + \left(L_m - \frac{L_1L_2}{L_m}\right)\boldsymbol{i}_{1,\alpha\beta} \tag{9}$$

For predictive control using a three-phase converter, considering the eight voltage vectors as combinations of the gating signals $S_a$, $S_b$ and $S_c$ as presented in Table 1.

Table 1. Switching States and Voltage Vectors

| $S_a$ | $S_b$ | $S_c$ | Vector Voltage $\boldsymbol{v}_1$ |
|---|---|---|---|
| 0 | 0 | 0 | $\boldsymbol{v}_1(1) = 0$ |
| 1 | 0 | 0 | $\boldsymbol{v}_1(2) = \frac{2}{3}V_{dc}$ |
| 1 | 1 | 0 | $\boldsymbol{v}_1(3) = \frac{1}{3}V_{dc} + j\frac{\sqrt{3}}{3}V_{dc}$ |
| 0 | 1 | 0 | $\boldsymbol{v}_1(4) = -\frac{1}{3}V_{dc} + j\frac{\sqrt{3}}{3}V_{dc}$ |
| 0 | 1 | 1 | $\boldsymbol{v}_1(5) = -\frac{2}{3}V_{dc}$ |
| 0 | 0 | 1 | $\boldsymbol{v}_1(6) = -\frac{1}{3}V_{dc} - j\frac{\sqrt{3}}{3}V_{dc}$ |
| 1 | 0 | 1 | $\boldsymbol{v}_1(7) = \frac{1}{3}V_{dc} - j\frac{\sqrt{3}}{3}V_{dc}$ |
| 1 | 1 | 1 | $\boldsymbol{v}_1(8) = 0$ |

The equations which relate the current derivative, rotor and stator flux derivative, with the parameters of the induction machine, as shown in (6), (7) and (8) (Rodriguez and Cortes, 2012).

$$\tau_\sigma\frac{d\boldsymbol{i}_{1,\alpha\beta}}{dt} = \frac{k_2}{R_\sigma}\left(\frac{1}{\tau_2} - j\omega\right)\boldsymbol{\lambda}_{2,\alpha\beta} + \frac{\boldsymbol{v}_{1,\alpha\beta}}{R_\sigma} - \boldsymbol{i}_{1,\alpha\beta} \tag{10}$$

$$\frac{d\boldsymbol{\lambda}_{1,\alpha\beta}}{dt} = \boldsymbol{v}_{1,\alpha\beta} - R_1\boldsymbol{i}_{1,\alpha\beta} \tag{11}$$

where:

$$k_2 = \frac{L_m}{L_2}$$
$$\tau_2 = \frac{L_2}{R_2}$$
$$\sigma = 1 - \left(\frac{L_m^2}{L_1L_2}\right)$$
$$R_\sigma = R_1 + k_2^2R_2$$
$$\tau_\sigma = \frac{\sigma L_1}{R_\sigma}.$$

The idea of the DTC is used for Predictive Torque Control but aims at the stator flux and torque futures values by predictive model. A cost function that considers the future behavior is used to implemented the reference signal,

which consist basically the electromagnetic torque and flux signal. Based on Table 1 the predictions solve the cost function for each voltage vectors, consequently, after obtain the optimal value of cost is selects the voltage vector that will be applied to the electrical machine to achieve the reference signal. To predict the future value of the electromagnetic torque and stator flux and must be discretized by the induction machines equations by a sampling time $T_s$. The derivation process is performed through forward Euler approximation as shown in (12).

$$\frac{dx}{dt} = \frac{x(k+1) - x(k)}{T_s} \tag{12}$$

Which is replaced in (5), (9), (10) and (11), then the expressions for each future state can be calculated by (13)-(17) for SCIM.

$$\widehat{\lambda}_1(k) = \widehat{\lambda}_1(k-1) + T_s \boldsymbol{v}_1(k) - R_1 T_s \boldsymbol{i}_1(k) \tag{13}$$

$$\widehat{\lambda}_2(k) = \frac{L_2}{L_m}\widehat{\lambda}_1(k) + \left(L_m - \frac{L_1 L_2}{L_m}\right)\boldsymbol{i}_1(k) \tag{14}$$

$$\lambda_1^p(k+1) = \widehat{\lambda}_1(k) + T_s \boldsymbol{v}_1(k) - R_1 T_s \boldsymbol{i}_1(k) \tag{15}$$

$$\begin{aligned}\boldsymbol{i}_1^p(k+1) = &\left(1 - \frac{T_s}{\tau_\sigma}\right)\boldsymbol{i}_1(k) + \\ &+ \frac{T_s}{\tau_\sigma}\left\{\frac{1}{R_\sigma}\left[\left(\frac{k_2}{\tau_2} - k_2 j\omega\right)\widehat{\lambda}_2(k) + \boldsymbol{v}_1(k)\right]\right\}\end{aligned} \tag{16}$$

$$T_e^p(k+1) = \frac{3}{2} N_p \Im m[\boldsymbol{\lambda}_1^*(k+1) \cdot \boldsymbol{i}_1^p(k+1)] \tag{17}$$

Where, $\widehat{\lambda}_1(k)$ and $\widehat{\lambda}_2(k)$ are the stator and rotor flux estimated.

In terms of voltage vector by Table 1 the predictions of flux and torque can be obtained. Then, the cost function (18) gives the control law according to the switching state that selects the vector that produces the lowest cost value.

$$g = |T_{eRef} - T_e^p(k+1)| + \lambda_\psi |\lambda_{1Ref} - \lambda_1^p(k+1)| \tag{18}$$

$\lambda_\psi$ is the weighting factor, which depending on your value it is used to balance the proportion between stator flux and torque. Fig.1 is a block diagram to represent the electrical scheme to the Predictive Torque Control and Table 2 are presented the parameters of the system.

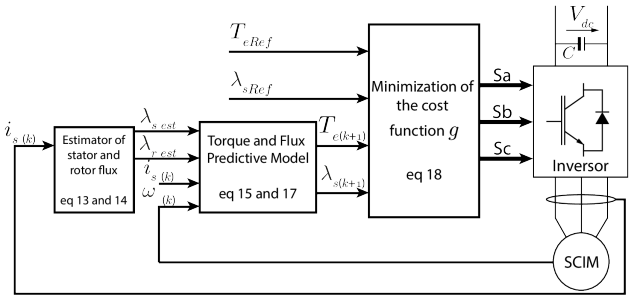


Figure 1. Block diagram for predictive direct torque control.

Table 2. System Parameters

| Parameter | Value | Quantity |
|---|---|---|
| DC Bus Voltage ($V_{dc}$) | 300 | ($V$) |
| Rated Torque | 16 | ($N.m$) |
| Number of Poles (2p) | 4 | poles |
| Rated Speed ($N_r$) | 1730 | rpm |
| Frequency | 60 | ($Hz$) |
| $R_s$ | 1,15 | ($\Omega$) |
| $L_s$ | 209,7 | ($mH$) |
| $R_r$ | 1,083 | ($\Omega$) |
| $L_r$ | 209,7 | ($mH$) |
| $L_m$ | 203,7 | ($mH$) |
| $J$ | 0,05 | ($kg.m^2$) |
| $f_{sw}$ | 6 | ($kHz$) |

## 3. SIMULATION RESULTS

The controller proposed must be validated through some computational software, for this paper we use the Matlab Simulink, which enables implement the mathematical model of SCIM. Moreover, electronic elements as IGBTs for the three-phase bridge, inductors for the filter, capacitors to keep the voltage of the DC link. The parameters of SCIM can be found in the appendix.

The signal test is a reference with variation between $-2Nm$ and $2Nm$ for torque and 0.3 $Wb$ and 0.4 $Wb$ for stator flux. Fig.2 and Fig.3 shows the simulation results.

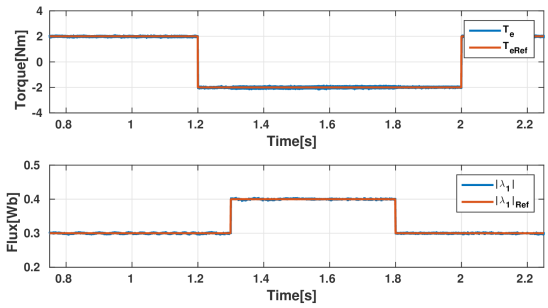


Figure 2. Simulation results for torque and stator flux test.

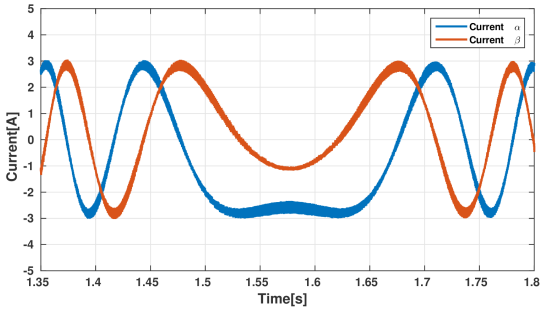


Figure 3. Simulation results for torque and stator flux test.

The figures presented before showing the measured signal as torque, flux and current oscillating around the reference, due to the limited number of vectors that the controller can choose. If the controller designer needs to reduce this oscillation, it is necessary to choose a higher sample frequency, in this paper was chosen approximately 16kHz to avoid distorting at the current. The sample frequency is not fixed because the type of controller, but the controller is capable to tracking the reference.

## 4. FINITE ELEMENT METHOD INVESTIGATION

The goal of finite element analysis is to obtain the flux density in the stator and rotor cores under a known value of rotor speed.

Based on the flux densities (Strous et al., 2016), it is possible to check undesirable levels of saturation, avoiding problems during the control system operation of the squirrel cage induction motor. The current and voltage injection in the stator and rotor are necessary, in order to keep the correct frequency and power to the grid, so that the stator is connected to the grid converter. Two simulations were carried out using two different values of current, 2.12 $A$ and 2.47 $A$, with voltages of 42.42 $V_{rms}$ and 33.95 $V_{rms}$ respectively. Both simulations with 12.5 Hz injected into the stator winding. The current, voltage and frequency values were obtained from tests in the prototype. Table 3 shows the prototype data of the prototype installed in LEPS (Laboratory of Renewable Energy and Power Electronics) at the Federal University of ABC (UFABC).

Table 3. Squirrel Cage Induction Machine Prototype Data

| Parameter | Value |
|---|---|
| Rated Power ($P$) - ($kW$) | 3 |
| Number of Phases | 3 |
| Number of Poles (2p) | 4 |
| Rated Speed ($N_r$) | 1730 |
| Armature Slots | 36 |
| Armature Winding | Double Layer |
| Coil Pitch - (slots) | 12 |
| Rated Armature Voltage - Y connection (V) | 220 |
| Rotor Slots | 27 |

## 5. MAGNETIC TRANSIENT FINITE ELEMENT METHOD SIMULATION

The transient simulation aims to evaluate the flux density in the core of the generator (Wang et al., 2015). The problem were elaborated with a constant speed (da Luz et al., 2002), as present in (19).

$$(\nabla \times \delta \nabla \times \boldsymbol{A}) - \boldsymbol{J} + \left(\sigma \frac{d\boldsymbol{A}}{dt}\right) + (\sigma \nabla V) + (\nabla \times \boldsymbol{Hc}) - (\sigma \nu \times \nabla \times \boldsymbol{A}) = 0 \quad (19)$$

In (19) the constants $\delta$ , $\sigma$ and $v$ are the reluctivity, electric conductivity and the speed in steady state, respectively. Also $V$ is the source scalar electric, $\boldsymbol{Hc}$ is the coercive force, which is zero in this case, since there are not permanent magnets, $\boldsymbol{J}$ is the conductors current density and A is the vector potential. Table 4 shows the quantities used in this simulation (Kumar et al., 2010).

Table 4. Simulation Data

| Parameter | Value |
|---|---|
| Scalar Electric Potential ($V$) | 42.42 - 33.95 |
| Operation Speed (rpm) | 335 |
| Grid Frequency ($Hz$) | 22,5 |
| Rotor Frequency ($Hz$) | 21,15 |
| Simulation Time ($s$) | 0,166 |
| Time Step | 0,0001 |

The generator has axial symmetry, taking advantage of this it is possible to formulate the problem with only half the geometry to use less memory available by the computer. Fig.4 and Fig.5 show in details the geometry used for simulation.

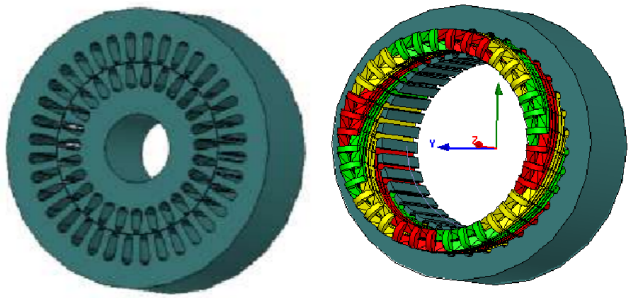

Figure 4. Detail of half of the Geometry and Armature Winding.

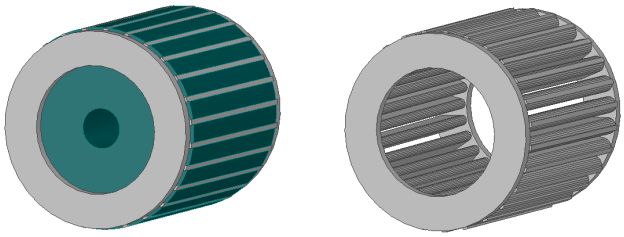

Figure 5. Detail of the Rotor Geometry and Skiewed Squirrel Cage.

Figure 6 illustrates the boundary conditions of the vector $\boldsymbol{A}$.

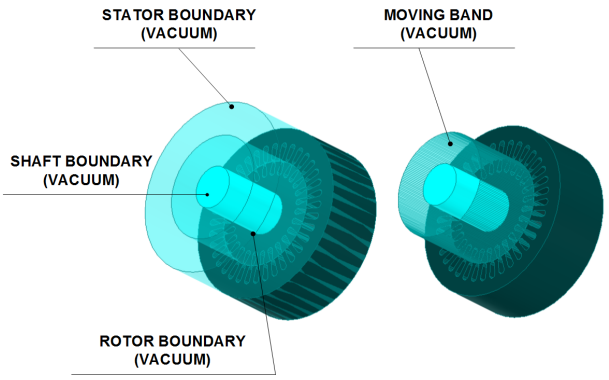


Figure 6. Specific boundaries, physical properties and moving band for magnetic transient analysis.

The stator and the rotor material used during the simulation step was the 1010 carbon steel in which its BH curve is presented in Fig.7.

It is possible to observe from the computational simulation, in Fig.8 and Fig.9, that the color map shows the levels of flux density in the stator and the rotor cores according to the conditions described previously.

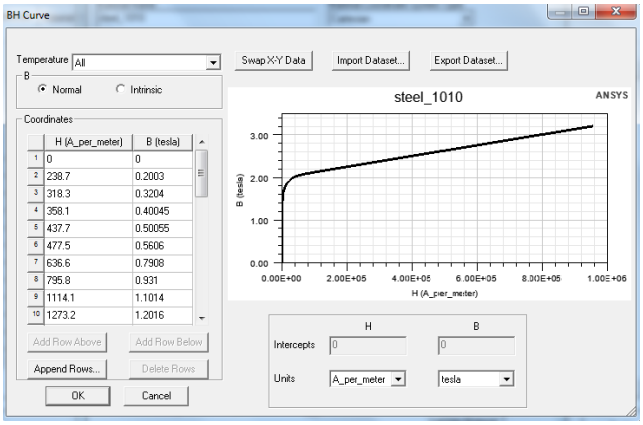


Figure 7. 1010 Carbon Steel BH Curve used in the armature and in the rotor.

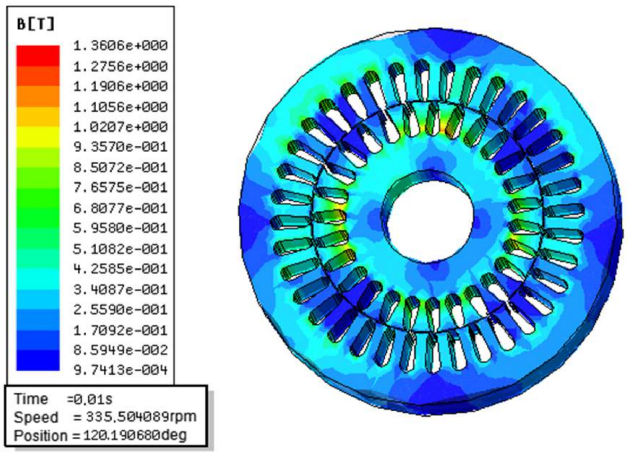


Figure 8. Flux Density at Rms current of 2.12 [$A$] in the stator with 335 [rpm].

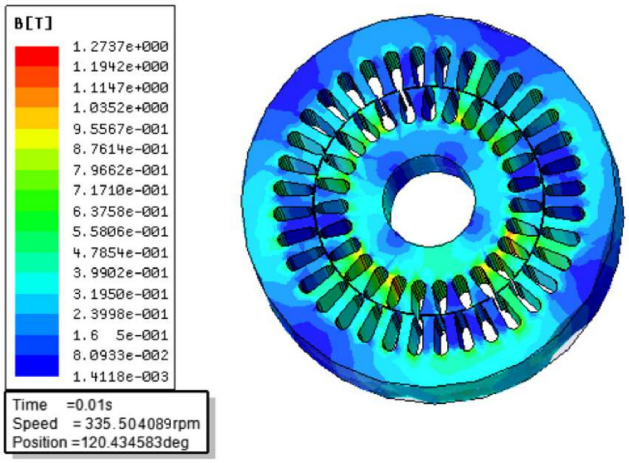


Figure 9. Flux Density at Rms current of 2.47 [$A$] in the stator with 335 [rpm].

Considering whole geometry, the flux densities got from the color maps were lower than the ferromagnetic material saturation point used which is about of 2.1 [$T$]. These results were obtained in both simulations, therefore, the control system can operate in a situation out of saturation point. The figure 10 illustrates the behavior of the control system against a torque step, and in the figure 11 shows the test bench.

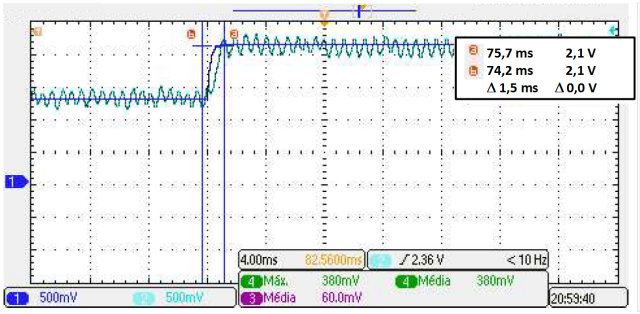


Figure 10. Response Control Behaviour.

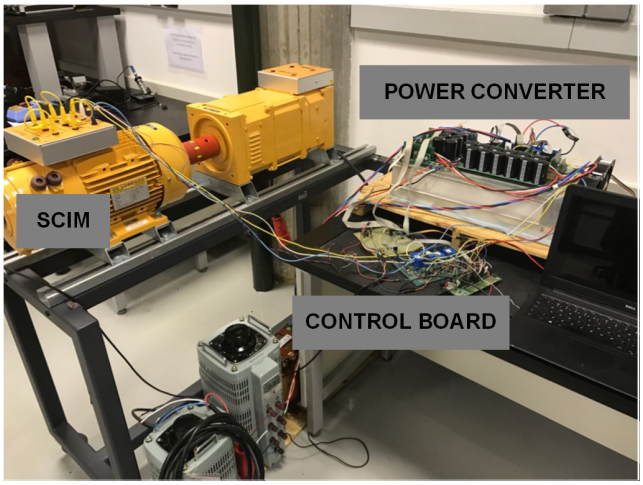


Figure 11. Bench Test View.

Through finite element analysis it was possible to verify previously the machine non-saturation condition, considering that the ferromagnetic core does not saturate, which enabled the implementation of the linear control proposed in the computational simulation and on the benchtest. Therefore, the benchtest validates the implementation of the software control of the dynamic model, being possible to notice that the controlled torque follows the reference torque value.

## 6. CONCLUSIONS

The main idea of this article is the application of the finite element study in electrical machines for operation with predictive controllers, mainly analyzing the saturation level in the core or other electromagnetic effects that occur in the machine being controlled. The simulations result of controller provides the magnitudes of current when applies a certain values of torque and flux, this results were used in the finite element software to obtain the knowledge of electromagnetic effects. The finite element analyses allow guaranteeing that the motor drive does not saturate the induction motor cores.

## REFERENCES

Abad, G., Lopez, J., Rodríguez, M., Marroyo, L., and Iwanski, G. (2011). *Doubly fed induction machine: modeling and control for wind energy generation*, volume 85. John Wiley & Sons.

Altuna, J.A.T., Jacomini, R.V., Puma, J.L.A., Capovilla, C.E., and Filho, A.J.S. (2015). Controlador deadbeat aplicado ao controle direto de torque do motor de indução trifásico. *Revista Eletrônica de Potência*, 20(3), 236–243.

Blaschke, F. (1972). The principle of field orientation as applied to the new transvektor closed-loop control system for rotating field machines.

Costa, F., Sguarezi Filho, A., Capovilla, C., and Casella, I. (2014). Morphological filter applied in a wireless deadbeat control scheme within the context of smart grids. *Electric Power Systems Research*, 107, 175–182.

da Luz, M.V.F., Dular, P., Sadowski, N., Geuzaine, C., and Bastos, J.P.A. (2002). Analysis of a permanent magnet generator with dual formulations using periodicity conditions and moving band. *IEEE Transactions on Magnetics*, 38(2), 961–964. doi:10.1109/20.996247.

Depenbrock, M. (1988). Direct self-control (dsc) of inverter-fed induction machine. *IEEE transactions on Power Electronics*, 3(4), 420–429.

Fiser, R. and Ferkolj, S. (2001). Application of a finite element method to predict damaged induction motor performance. *IEEE Transactions on Magnetics*, 37(5), 3635–3639.

Hernandez Navas, M.A., Azcue Puma, J.L., and Sguarezi Filho, A.J. (2015). Direct torque control for squirrel cage induction generator based on wind energy conversion system with battery energy storage system. In *Power Electronics and Power Quality Applications (PEPQA), 2015 IEEE Workshop on*, 1–6. IEEE.

Holtz, J. and Stadtfeld, S. (1983). A predictive controller for the stator current vector of ac machines fed from a switched voltage source. In *Proc. IPEC*, 1665–1675.

Holtz, J. (1994). The induction motor-a dynamic system. 1, P1–P6.

Kennel, R. and Linder, A. (2000). Predictive control of inverter supplied electrical drives. In *Power Electronics Specialists Conference, 2000. PESC 00. 2000 IEEE 31st Annual*, volume 2, 761–766. IEEE.

Kumar, A., Marwaha, S., Marwaha, A., and Kalsi, N. (2010). Magnetic field analysis of induction motor for optimal cooling duct design. *Simulation Modelling Practice and Theory*, 18(2), 157–164.

Rodriguez, J. and Cortes, P. (2012). *Predictive control of power converters and electrical drives*, volume 40. John Wiley & Sons.

Rodriguez, J., Pontt, J., Silva, C., Kouro, S., and Miranda, H. (2004). A novel direct torque control scheme for induction machines with space vector modulation. In *Power Electronics Specialists Conference, 2004. PESC 04. 2004 IEEE 35th Annual*, volume 2, 1392–1397. IEEE.

Sahraoui, M., Ghoggal, A., Zouzou, S.E., and Benbouzid, M. (2008). Dynamic eccentricity in squirrel cage induction motors–simulation and analytical study of its spectral signatures on stator currents. *Simulation Modelling Practice and Theory*, 16(9), 1503–1513.

Sguarezi Filho, A.J. and Ruppert, E. (2010). A deadbeat active and reactive power control for doubly fed induction generator. *Electric Power Components and Systems*, 38(5), 592–602.

Silva, S.A.O.D., Santos, T.H.D., Goedtel, A., and Suetake, M. (2014). Controle escalar do motor de indução usando a técnica sensorless neural. *Revista Eletrônica de Potência*, 19(1), 024–035.

Strous, T.D., Wang, X., Polinder, H., and Ferreira, J.A. (2016). Saturation in brushless doubly-fed induction machines. In *8th IET International Conference on Power Electronics, Machines and Drives (PEMD 2016)*, 1–7. doi:10.1049/cp.2016.0274.

Takahashi, I. and Noguchi, T. (1986a). A new quick-response and high-efficiency control strategy of an induction motor. *IEEE Transactions on Industry applications*, (5), 820–827.

Takahashi, I. and Noguchi, T. (1986b). A new quick-response and high-efficiency control strategy of an induction motor. *IEEE Transactions on Industry applications*, (5), 820–827.

Vitorino, M.A., de Rossiter Corrêa, M.B., Jacobina, C.B., and Lima, A.M.N. (2011). An effective induction motor control for photovoltaic pumping. *IEEE Transactions on Industrial Electronics*, 58(4), 1162–1170.

Wang, X., Strous, T.D., Lahaye, D., Polinder, H., and Ferreira, J.A. (2015). Finite element modeling of brushless doubly-fed induction machine based on magnetostatic simulation. In *2015 IEEE International Electric Machines Drives Conference (IEMDC)*, 315–321. doi:10.1109/IEMDC.2015.7409077.

Yazdani, A. and Iravani, R. (2010). *Voltage-sourced converters in power systems: modeling, control, and applications*. John Wiley & Sons.